A View-independent Line-Coding Colormap for Diffusion Tensor Imaging

Wu, Shin-Ting[a], Raphael Voltoline[a], Clarissa Lin Yasuda[b]

[a] School of Electrical and Computer Engineering, University of Campinas, Campinas, Brazil
[b] School of Medical Science, University of Campinas, Campinas, Brazil

Abstract

Diffusion Tensor Imaging is a noninvasive technique promising for assessing the integrity of white matter tracts in the brain through the measurement of the movement of water. Because of the dimensions of the data involved, visualization of slice-by-slice images is still a challenge, and the colormaps for conveying the spatial direction of the major eigenvector of the diffusivity tensors widely adopted are ambiguous. The present paper addresses the issue of how to ameliorate this ambiguity. We propose a new line-coding color scheme, contemplating human visual perception in conjunction with the classic Hue-Saturation-Value color model. Experiments with neuroimages were also conducted to assess the potential of the proposal in the perception of spatial orientations in 2D views.

Keywords: Structural brain abnormalities visualization, Diffusion tensor imaging, Line-coding colormap

1. Introduction

The use of diffusion-weighted magnetic resonance images (DW-MRI) is a well-established technique for the estimation of the diffusivity of water in living tissues. This diffusion is anisotropic in organized tissues such as muscles and the white matter of the brain [1]. The introduction of diffusion tensor imaging (DTI) models has made it possible to describe this diffusivity in a way that is invariant, independent of rotation. Since its development, DTI has been applied in the investigation of various cerebral tract structures; this has increased the potential for the diagnosis of diverse neurological disorders [2]. The appropriate visualization of DTI images provides a potential technique for revealing the complex structure of the cerebral white matter in an understandable way [3].

In DTI the estimated diffusivity of a scanned sample is represented by a second-order tensor (3×3 matrix). Providing an integrated, but visually distinguishable, representation of all nine elements of each tensor is, however, not a trivial task. Kindlmann proposes superquadric functions for visualizing the tensors as spatial glyphs [4]. Since they can obscure each other, however, such glyphs fail to convey complex 3D fiber tracts. Fortunately, for most anatomical and functional studies, only the streamline of strongest diffusion is of interest, and the nine-element tensor visualization can be reduced to that of a single three-element vector. Such vectors can be used to construct 3D (hyper)streamlines with use of tractography [5, 6]. The result of this technique, however, is very sensitive to user input, and important information can be missed if the underlying anatomy is not known [7]. Furthermore, spatial paths are usually difficult to visualize from 2D images.

Slice-by-slice investigation is still the dominant practice among radiologists for the diagnosis of abnormalities [8]. In these 2D views of the slices, each sample can be viewed fully, thus allowing precise exploration and analysis. Multimodality can enhance visualization for diagnosis, but this requires the unambiguous mapping of the fiber orientation onto some sort of graphics attribute to be displayed with other imaging modalities in order to improve the sensitivity and specificity of a 2D visual inspection protocol. Since 2D visual inspection continues to be used, the representation of both color and space in three dimensions can facilitate the portrayal of the vector fields as colors.

One of the uses of the measures of DTI is the identification of the paths of white matter tracts (line path), rather than a vector field of water diffusion (vector direction) [1]. Hence, in the visualization of DTI images, two co-linear vectors of opposite directions should be indistinguishable. Pajevic and Pierpaoli call such DTI data axial data, and they carefully compare the known Hue-Saturation-Value (HSV)-based color schemes in relation to the three main sources of misinterpretation: discontinuity artifacts, human perceptual distortions, and ambiguity in orientation. They conclude that none of the color schemes studied is free of misinterpretation. Figure 1 provides an example of the use of the HSV color scheme showing a unique representation, but suffering from discontinuity along the equator if the viewing angle is not restricted to less than 90^o [9]. Figure 1(b) illustrates this discontinuity at the equator of a sphere with the points in the immediate vicinity mapped onto antipodal points. To illustrate this, Figure 1(b) presents these antipodal points in a rectangular coordinate system, with the vectors (x, y, z) presented as a solid line while -(x, y, z) is dashed.

In this paper we present a novel color scheme which facilitates interpretation, while still perceptually satisfying the requirements of continuity and non-ambiguity. The key to this proposal is the exploration of smooth transitions between primary and secondary colors in the classic RGB color model. In Section 2 we compare the results of different color coding schemes in the visualization of DTI images. The proposed so-

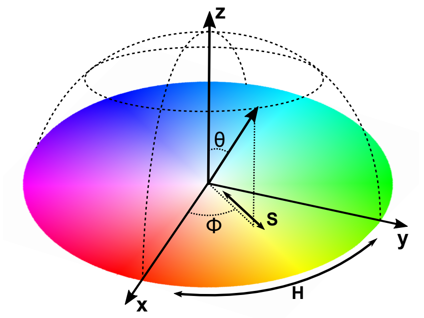

(a)

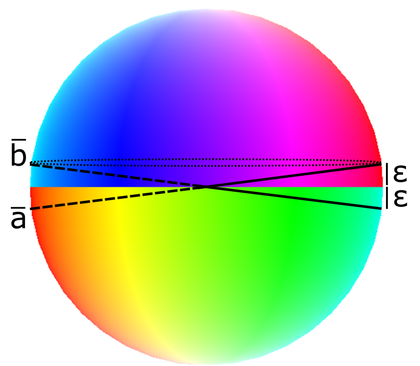

(b)

Figure 1: *HSV* mapping: (a) one-to-one mapping between color parameters (H,S) and the spherical coordinates (ϕ,θ), and (b) discontinuity artifact on equator of the color sphere.

lution is detailed in Section 3, and in Section 4 various experiments performed to assess the effectiveness of the proposed scheme in conveying information about the trajectory of neural tracts are outlined. The limited difference of this color mapping in relation to that observed in previous research makes this option seem promising, as discussed in Section 5. Finally, some concluding remarks are made in Section 6.

2. Related Work

Color-mapping is a useful and widely accepted technique for visualizing specific 3D vector fields, such as normal vectors [10] and the flow of fluids in computational fluid dynamics [11]. Since the seminal work of Pajevic and Pierpaoli [9], just a few suggestions of schemes for coloring DTI data using vector coding have been published. The main ideas presented have been summarized in this section.

According to Pajevic and Pierpaoli, four requirements are necessary in the design of a colormap for displaying fiber orientation: (1) linearity in color perception; (2) the reference system for describing orientation; (3) the establishment of a threshold for displayable anisotropy; and (4) the interpretability of the colors used. The first requirement is related to the use of color variation to indicate variations in vector direction. Vectors with similar directions should be portrayed by similar colors, with the difference between the colors becoming perceptually greater as the angle between the directions increases. The second requirement concerns the reference system of the color space, which should be invariant with respect to the angle of viewing, generally considered to be the orthogonal coordinate system of the patient. The third requirement refers to the common practice of modulating the color value by the anisotropy of diffusion, so that a sample becomes less visible as its isotropy decreases, a practice that can reduce visual pollution. The final one involves the mental inversion of color-mapped directions.

Each normalized 3D vector (x, y, z) in a patient's coordinate system must be unambiguously mappable to a distinct point on the unit sphere. Moreover, the vectors (x, y, z) and $-(x, y, z)$ must be mapped on the same color. Then, a single hemisphere of spherical coordinates (ϕ, θ) must be sufficient to represent all fiber orientations. Color coding of the spherical coordinates for such a point on a single hemisphere is possible if the *HSV* color model is used (Figure 1): the azimuthal angle ϕ and the polar angle θ of the direction of a fiber at each point are associated with a specific color hue (H) and the color saturation (S), respectively, through the following formula:

$$H = (\phi - \phi_R + 2\pi)\ mod\ 2\pi \quad S = \sin(\theta), \tag{1}$$

where $(\phi_R, \frac{\pi}{2})$ is the orientation of the spatial line that is mapped onto saturated red. For simplicity, the color value (V) is set at 1.0. Since ϕ_R is an arbitrary angle, modular arithmetic is adopted to avoid a negative H value: 2π is added to the difference $(\phi - \phi_R)$, and the result is wrapped around 2π. This mapping, denominated non-symmetrical color coding, is considered user-friendly, as it mimics the way an artist mixes paints on his palette [12]. Moreover, it does not suffer from ambiguity in orientation. However, it gives rise to color discontinuity artifacts, due to the mapping of two crossing lines, $\overline{a} = (\phi, \frac{\pi}{2} - \epsilon)$ and $\overline{b} = (\phi, \frac{\pi}{2} + \epsilon)$, on two distinct antipodal points in the *HSV* color space ($(\phi, \frac{\pi}{2} - \epsilon)$ and $(\phi + \pi, \frac{\pi}{2} - \epsilon)$). In Figure 1(b) these two antipodal points lie on the dotted circle parallel to the equator. To overcome this discontinuity problem, preferred direction mapping is used.

Preferred direction mapping consists of applying non-symmetrical mapping on a unit sphere having its poles aligned in the preferred direction. Schlüter et al. propose the establishment of this direction in a way that automatically shifts the discontinuity artifacts. They define the preferred direction as the normal vector of the plane for which the average distance between the major diffusivity direction of each sample and its projection onto a plane is minimal [13]. This plane is called the optimal projection plane. Höller et al. map the angle between the average anisotropic diffusion direction and the vector perpendicular to the displayed slice onto the hue of the Hue-Saturation-Brightness (*HSB*) color model. The major shortcoming of the two preferred direction coding schemes, however, are that they violate the requirement of viewing invariance. Three other schemes for mapping have also been investigated in [9]: absolute value, rotational symmetry and mirror symmetry.

Absolute value mapping maps the absolute values of the ele-

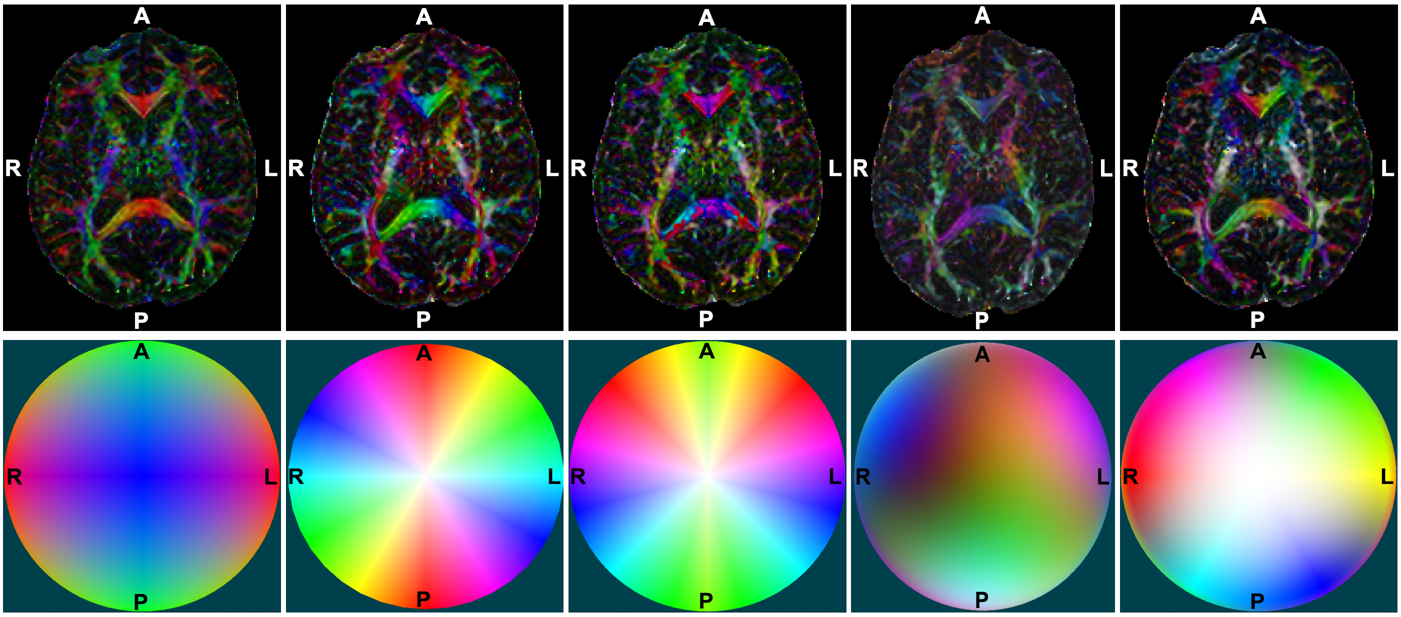

(a) (b) (c) (d) (e)

Figure 2: Different line-coding color schemes to represent the orientation of white matter fibers for each sample: (a) absolute value (conventional), (b) rotational symmetry, (c) mirror symmetry, (d) Boy surface immersion, and (e) the proposed color scheme. The DTI images showing color-coded orientation and the corresponding color coding schemes are shown in the top and the bottom row, respectively.

ments of fiber orientation (x, y, z) onto color elements, i.e.

$$R = |x| \quad G = |y| \quad B = |z|.$$

This color scheme has been found useful for displaying fiber tracts in axial slices, since it facilitates the discovery of the large asymmetries between the left and right hemispheres which provide evidence of abnormalities [14]. One example of this color coding is shown in the visualization of axial diffusion data in Figure 2(a). Note that there is no color discontinuity in regions where the variation in orientation is smooth, but there is a serious problem with ambiguity in spatial orientation. It is not possible, for example, to discern the difference in orientation of the commissural fibers in the left and right brain hemispheres.

Rotational symmetry mapping was designed to guarantee that any vector and its inverse are mapped onto the same color, i.e.

$$H = (2(\phi - \phi_R + 2\pi)) \ mod \ 2\pi.$$

Figure 2(b) shows how the ambiguity in orientation has been perceptually ameliorated, although not completely eliminated.

Mirror symmetry mapping was designed to portray any vector and its mirror image with respect to the midsagittal plane in the same color code, i.e. the azimuthal angle $\phi \in [0, \frac{\pi}{2}] \cup [\frac{3\pi}{2}, 2\pi]$ for each direction $(|x|, y, z)$ is mapped onto the specific hue using the following equation

$$H = 2((\phi - \phi_R + \pi) \ mod \ \pi).$$

Although mirror symmetry can be extremely helpful for highlighting differences between the left and right brain hemisphere, the mapping presents problems of ambiguity in orientation, as well as of discontinuity, as illustrated in Figure 2(c).

The color coding scheme proposed by He et al. was designed to maximize the use of the color space and reduce discontinuity artifacts [15]. These authors seem to resize and displace the direction vectors to the vectors in the first octant of the cartesian coordinate system, then to map the new vectors onto the RGB color cube; however, the fact that no key to the color mapping is provided in their paper and that the colors used are not familiar to neuroradiologists makes the interpretation of the images included in the paper quite difficult. It seems, however, that the proposed scheme satisfies the following unit vector (x, y, z) onto color (R, G, B) mapping rule:

$$R = \frac{x/2 + 0.5}{2} \quad G = \frac{y/2 + 0.5}{2} \quad B = \frac{z/2 + 0.5}{2}.$$

If this inference is correct, the scheme maps a vector (x, y, z) and its inverse $-(x, y, z)$ on two distinct colors, although this is not desirable for representing the pathways of fiber bundles.

The final color scheme presented is that proposed by Demiralp et al. for tackling the discontinuity problem on the equator of a sphere [16]. The key to their proposal is two-dimensional real projective space (RP^2), which consists of the set of all lines in R^3 passing through the origin. This space is topologically equivalent to the unit sphere S^2 where every point and its antipodal point are not distinguished, and can be further restricted to the upper hemisphere with the antipodal points at the equator "glued together". There are some known immersions of RP^2 in R^3: Boy surface, cross-cap and Roman surface.

Representing line paths in RP^2, Demiralp et al. propose a "piecewise linear version of Boy's surface" to map the line path in the rectangular coordinates (x, y, z) onto the coordinates

$(f_1(x,y,z), f_2(x,y,z), f_3(x,y,z))$ of the *RGB* color space. This scheme first evaluates the function $g_j(x,y,z)$, $j = 1,2,3$, written as a partial weighted sum of $n+1$ spherical harmonics

$$g_j(x,y,z) \approx \sum_{i=0}^{n} c_{ji} h_{ji}(x,y,z) \tag{2}$$

with $h_{ji}(x,y,z)$ and c_{ji} denoting the spherical harmonics and real-valued weights, respectively. Then, it scales and normalizes $(g_1(x,y,z), g_2(x,y,z), g_3(x,y,z))$ to get a point on the RGB space. It should be noted that some coefficients in Eq. 2 were adjusted by hand to achieve an aesthetically pleasing shape. An example implementation in Python is available online at [17].

The elegance of the underlying mathematical formulation of the color coding scheme proposed by Demiralp et al. and the generally unambiguously smooth mapping make the scheme extremely appealing, although there is a set of self-intersections due to R^3 realization. Nevertheless, inverse mapping from the colors onto the line paths constitutes a problem. As can be seen in Figure 3, it is not a trivial task to sequence the colors surrounding each reference axis to effectively convey variations in θ and ϕ in the Left-Posterior-Superior (LPS) patient reference system, i.e. x-axis for the patient's L(eft) side, y-axis for the patient's P(osterior) side and z-axis for the patient's S(uperior) side [18]. Hence, fibers that have very similar spatial orientations may be colored with perceptually distinct colors, as is the case with the corticospinal tract in Figure 2(d). This does not comply with the requirement of linearity in color perception.

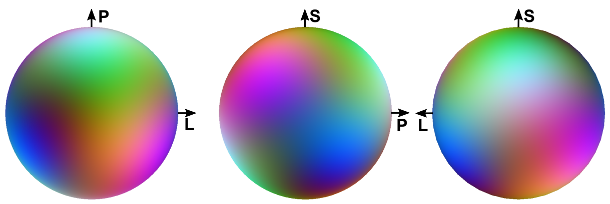

(a) (b) (c)

Figure 3: Orthogonal view of the Boy surface immersion color sphere in the direction of (a) S-axis, (b) L-axis and (c) P-axis.

Contributions The proposed alternative line-coding color scheme ameliorates ambiguity in orientation and visual discontinuity, thus facilitating the interpretation of DTI images, and it is useful in the more precise identification of the main direction of asymmetric water diffusion. Similar to the work of Demiralp et al. [16], this scheme presents a relatively unambiguous, smooth mapping between spatial orientations and colors. Instead of elegant but complex functions however, the present proposal relies on familiar color sequences and simple linear interpolation, thus facilitating the identification of spatial orientation from colors.

3. Proposal

Pajevic and Pierpaoli have noted that the main issue in unambiguous vector coding is the appearance of discontinuity [9]. Although the color wheel of the *HSV* color model can be easily interpreted and is familiar to most users, the discontinuity artifact due to discontinuity in the mapping in the vicinity of the equator can lead to misleading interpretations. Pajevic and Pierpaoli have also determined that perceptually uniform color spaces, within which the difference between the perception of two colors is proportional to their Euclidean distance, is not a solution, since that uniformity is limited when applied to color images. A huge number of color contrasts and discontinuity effects are known to influence visual experiences, but not because of perceptual non-uniformity. The illusion produced can even be an advantage and help reveal details and hidden information [19]. This background led us to look at the problem from a different angle, and the question was reformulated. Is it possible to remedy the flaws of *HSV*-based color codes without forfeiting their positive contributions?

The first idea was to change the position of the colors on the *HSV* color wheel so that the antipodal point of a primary color would become a secondary one, differing in respect to a single color element. This guarantees that a sequence of primary–secondary–primary–secondary–primary–secondary colors is established with respect to the angle ϕ of line orientations and that the saturated hue transition is similar to that observed in the *HSV*-based color scheme.

However, it is clear in Figure 6(a) that the problem of the color discontinuity at the equator of the sphere remains. It thus seems reasonable to move the colors away from the equatorial borders of the hemispheres to a northern meridian and a southern meridian by λ degrees, with the interpolated colors of the hemisphere borders used to represent the lines that cross in the vicinity of the equator of the sphere to produce smooth perceptual transitions. Nevertheless, a little reflection shows that this approach will require certain additional modifications. Simple interpolation of arbitrary colors may result in many achromatic values, and a patient's coordinate axis orientations may become perceptually indistinguishable.

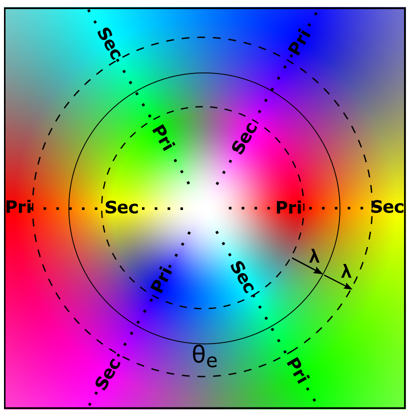

Figure 4: Proposed colormap without discontinuity artifact: arrangement of primary (Pri) and secondary (Sec) colors in stereographic projection.

It should be noted that in the present proposal the view-independent color codes for the patient's reference axis orientations are no longer the usual red, green and blue hues presented in Figure 2(a). We show the new colors for the reference axes, and suggest the adoption of a color weighting strategy to reduce visual pollution.

3.1. Color Wheel

The proposal presented here involves a modification of the spacing of colors around the color wheel. The primary and secondary colors on the border of the color wheel are equally spaced, counterclockwise, in the sequence red $(1, 0, 0)$, magenta $(1, 0, 1)$, green $(0, 1, 0)$, yellow $(1, 1, 0)$, blue $(0, 0, 1)$, and cyan $(0, 1, 1)$. This order is arbitrary, requiring only that, for each saturated color, (a) one of its adjacent colors differs from it in a single color element, while the other differs in three, and (b) the color of the antipodal point differs by a single color element.

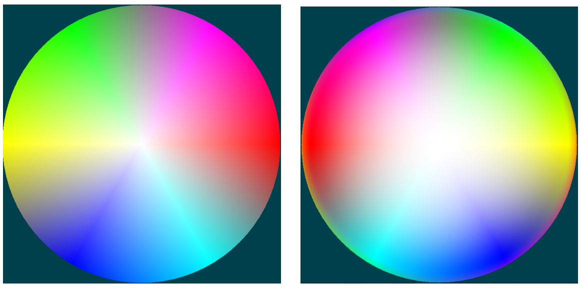

(a) (b)

Figure 5: Combination of primary and secondary colors on the color wheel, in parallel projection, with different exponents of the saturation: (a) $n = 1$ and (b) $n = 2$.

Since the adjacent colors can differ in either one or three color elements, only two rules for interpolation are necessary. When two colors differ in respect to a single color element c, linear color variation is possible only from the color element $c = 0.0$ to the color element $c = 1.0$. When they differ in three elements (c_1, c_2, c_3), the pattern variation is: one color element c_1 varies linearly from 0.0 to 1.0 and the other two elements c_2 and c_3 also change linearly, but in the opposite direction, from 1.0 to 0.0. From this interpolation, three samples along the equator will be mapped onto light gray $(0.5, 0.5, 0.5)$. However, color contrast effects will give the illusion of being different colors, as will be discussed in Section 5.

Applying this colormap to the DTI images showed that, because of the contrast effect, the line parallel to the reference z-axis (coded in white) is almost indistinguishable in complex structures. This probably reflects the fact that our visual perception is one-third less sensitive to chromatic than to achromatic variations, and it is highly dependent on the surrounding colors [19]. To mitigate this perceptual limitation, the saturation of the color in the vicinity of the z-axis was reduced. Instead of Eq. 1, the color saturation is redefined as:

$$S = \sin(t^n * \theta_e), \tag{3}$$

where n is the exponent of the saturation and t, the saturation factor, given by

$$t = \begin{cases} \frac{\theta}{\theta_e - \lambda}, & \theta \leq (\theta_e - \lambda) \\ 1, & \text{elsewhere} \end{cases},$$

where θ_e and λ are, respectively, the polar coordinate of the equator of the sphere and the interpolation range, as will be discussed in Section 3.2.

Figure 5 shows the difference in the colormaps generated with the exponent of saturation $n = 1$ (a) and with $n = 2$ (b). In this paper, all DTI slices are rendered with $n = 2$.

3.2. Linear Interpolation

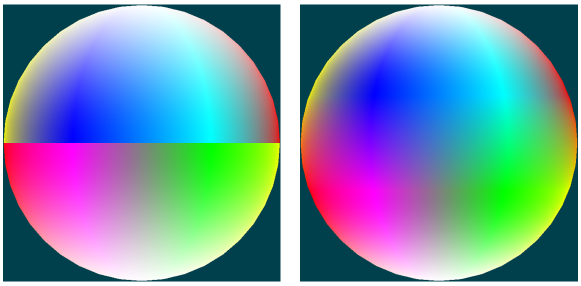

(a) (b)

Figure 6: Interface of two orientation hemispheres: (a) without and (b) with the interpolation belt on the equator.

With respect to the sphere equator, depicted as a solid circle in Figure 4, the adjacent colors located in the two different hemispheres differ in a single color element. Even so, however, the transition between them is not perceptually smooth, as shown in Figure 6(a). To remedy this problem, a transition belt on the two sides of the equator is defined between $\theta_e - \lambda$ and $\theta_e + \lambda$, with θ_e being the polar coordinate of the equator. In Figure 4 this region is bounded by the dashed circles. The colors on the displaced border of the northern hemisphere and those on the displaced border of the southern hemisphere are located in the inner and the outer dashed circles, respectively. The colors in the belt bounded by these two dashed circles are interpolated in a way analogously to what was done with the adjacent colors on the color wheel: if the values of the color elements of two colors are different, the color between them is subjected to linear interpolation, thus resulting in a smooth transition. Figure 6(b) shows the result of interpolation for $\lambda = 20^o$.

3.3. Axis Orientation

The color code for the orientation of the reference axis is crucial in the interpretation of color. To be view-independent, the reference system is generally aligned with the LPS-patient system. As already explained in Section 3.1, the line parallel to the z-axis, the S-axis, is coded in white (Figure 7(a)). Both the line parallel to the L-axis and that parallel to the P-axis are color-coded along the equator of the color sphere (Section 3.2). In the proposed scheme, the L-axis is represented by a shade of orange (the interpolation of red and yellow, corresponding to the displaced border colors at $\phi = 0$), and the P-axis by a shade of blue (the interpolation of the displaced border colors at $\phi = 90^o$). In Figure 7(b) the color sphere is rotated so that the point corresponding to the L-axis is located in the center of the color disc, while in Figure 7(c) this central point represents the P-axis.

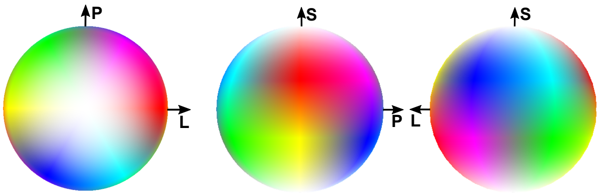

(a) (b) (c)

Figure 7: Orthogonal view of the color sphere in the direction of (a) S-axis, (b) L-axis and (c) P-axis.

3.4. *Encoding Anisotropy of Diffusion*

As mentioned in Section 2, it is common to weight the color vector by a scalar value characterizing diffusion. This scalar value can be the fractional anisotropy (FA) [20], which lies in the interval $[0.0, 1.0]$. When using FA to weight a color, the lower the FA, the darker the sample color is, with a decrease in FA from 1.0 to 0.0 resulting in a diminished hue. Therefore, nearly isotropic samples are either dark gray or black in color, and they are perceptually filtered out against a black background. This is the simplest way to highlight neural fibers. This filtering technique has been applied for all the DTI slices presented in this paper.

4. Experiments

The proposed color coding scheme was evaluated with diffusion data in relation to effectiveness in conveying the major neural tracts and its potential clinical value. This section presents the results from the data volumes of a healthy volunteer, as well as those of patients with neural disorders. The DTI images used here were obtained from DW-MRI images with 70 axial slices of 256×256. They were acquired with a Philips Achieva 3T Scanner using a spin-echo echo-planar diffusion-weighted sequence, 32 diffusion-encoding gradients, and a b-value of 1000 s/mm^2. The DW-MRI data acquired were processed using the FSL Diffusion Toolkit [21]. Because the raw data are in the format of Digital Imaging and Communications in Medicine (DICOM) [22], they were converted to the NIfTI format with dcm2nii software [23]. It should be noted that all subjects enrolled in the present study signed the informed consent form approved by the Ethics Committee of our university.

To assess the power of the proposed color scheme for clarity in the visualization of the line path, a study was made of certain tracts that are frequently studied with DTI images to compare those created applying the most frequently used absolute values with those based on the proposed color scheme (Figures 8–10). The original study of Pajevic and Pierpaoli had already compared the results of absolute values to those of other color schemes [9]. In Figures 8–10 the slices in the top row are colored with the traditional absolute value color scheme, whereas in the bottom row the same slices are rendered using the scheme proposed here.

Figure 8 shows the colormap of the major commissural fiber system, the corpus callosum, which connects the two cerebral

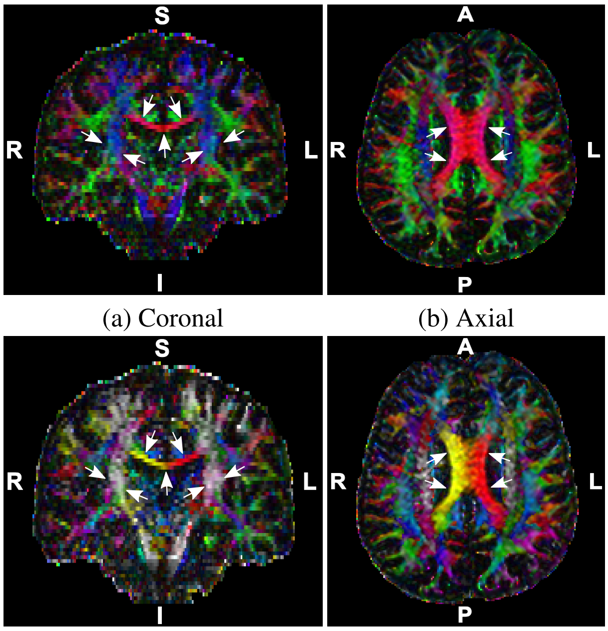

(a) Coronal (b) Axial

(c) Coronal (d) Axial

Figure 8: Comparison of fiber tracts in the corpus callosum, colored using absolute value (top row) and the proposed scheme (bottom row).

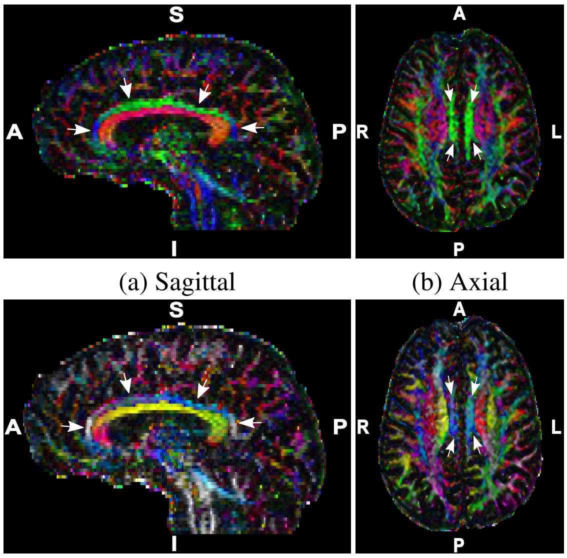

(a) Sagittal (b) Axial

(c) Sagittal (d) Axial

Figure 9: Comparison of fiber tracts in the cingulum, colored using absolute value (top row) and the proposed scheme (bottom row).

hemispheres in a right-to-left orientation, as well as the corticospinal tracts. The leftmost column and the rightmost one illustrate, respectively, coronal slices with the corticospinal tracts and axial slices with the maximum anterior-to-posterior width of the corpus callosum (indicated by the white arrow). Despite the low acquisition resolution along the axis from feet to head, which made angular variations difficult to distinguish in the coronal slice, the corticospinal tracts, in the shade of blue in the absolute value color scheme (Figure 8(a)), are more clearly revealed by the whitish color in Figure 8(c) with the present scheme. Moreover, the extremes of the corpus callosum bend up toward the patient's superior side, but the orientation of the two is different. This can been seen in the transitional orange of the present scheme (Figures 8(d)) located between the red indicating fibers running to the upper left and the yellow for those running to the upper right, in contrast to the single shade of red in the absolute color scheme (Figure 8(b)). It is remarkable that the ambiguities in orientation revealed in Figure 8(b) have been eliminated, as indicated by the white arrows in Figure 8(d).

Figure 9 shows the colormap of the cingulum (indicated by the white arrows). The left and the right columns present, respectively, sagittal and axial slices, showing the maximum anterior-to-posterior width of the cingulum. The cingulum is a collection of white matter fibers projecting from the cingulate gyrus to the entorhinal cortex. It is C-shaped, wrapping the corpus callosum from the frontal lobe to the temporal lobe. The continuous variations in colors are difficult to perceive in the absolute value scheme (Figures 9(a) and (b)). But, in the proposed scheme, we can see from Figures 9(c) and (d) that the fibers run in an anterior-to-posterior direction, with the inferior-to-superior directions varying gradually (from a superior orientation (white), to posterior-and-superior (grayish magenta) and then to anterior-and-inferior (light blue)). These colors can be seen to vary smoothly along the path from white to light blue. This produces the perception that the tract curves continuously along the path, even given the low resolution of the sagittal slice.

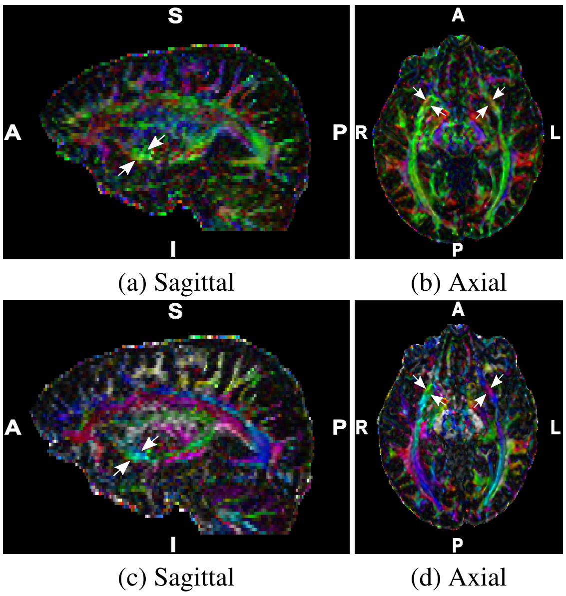

Figure 10: Comparison of fiber tracts in the uncinate fasciculus, colored using absolute values (top row) and those of the proposed scheme (bottom row).

Figure 10 shows the uncinate fasciculus, which is a white matter tract that connects the hippocampus and amygdala in the temporal lobe to the frontal lobe. It is a hook-shaped bundle running in an anterior-to-posterior orientation. Sagittal and axial slices colored with the two color schemes are portrayed in the left- and right-hand columns of the figure. In the two color schemes, the tracts are barely visible. In the slices colored using the absolute values (Figures 10(a) and (b)), this tract is displayed with a shade of greenish orange, while with the proposed scheme (Figures 10(c) and (d)), the origin lateral to the amygdala and hippocampus in the temporal lobe is seen to curve upward behind the external capsule and inward along the insular cortex (bluish shade), then up into the posterior part of the orbital gyrus (a shade of magenta). The white arrows in Figure 10 indicate this anatomic structure.

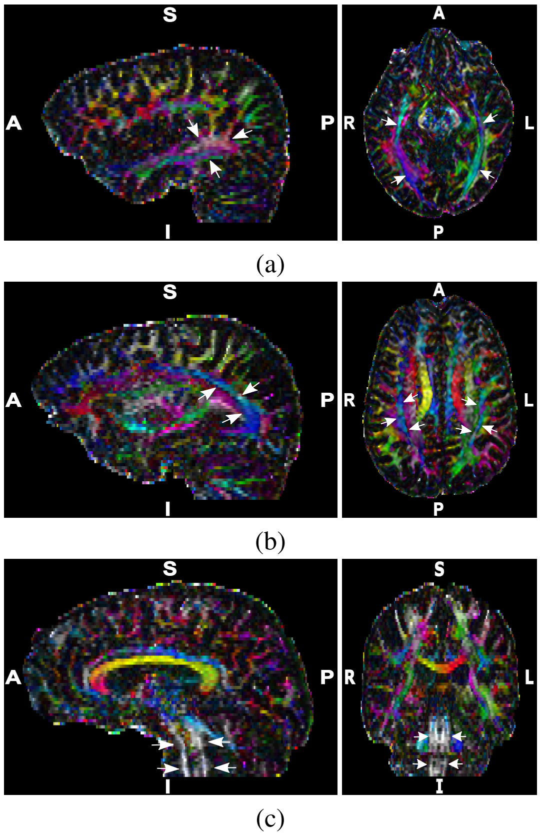

Figure 11: Three major neural tracts: (a) inferior, (b) superior longitudinal fasciculus; and (c) corticospinal tract.

The next visualization shows the orientation of three major neural tracts with the proposed color scheme: the inferior and the superior longitudinal fasciculi and the corticospinal tracts. The inferior longitudinal fasciculus consists of a pair of tracts that run along the lateral ventricle, connecting the occipital and the temporal lobes, while the superior longitudinal fasciculus connects the front and back of the cerebrum. The corticospinal tract runs longitudinally. The white arrows in Figures 11 highlight the structures of interest. The tracts of the inferior longitudinal fasciculus reveal mirror symmetry, but not exactly parallel; the left bundle is coded in a shade of bluish green while the right-hand bundle is in cyanish magenta (Figure 11(a)). Since the bundles of the superior longitudinal fasciculus are almost parallel to the cingulum along its entire course; they are coded throughout in the same bluish shade as the cingulum. This can be seen in Figure 11(b). In Figure 11(c) the corticospinal tract is colored white, corresponding to the orientation of the spinal cord from feet to head.

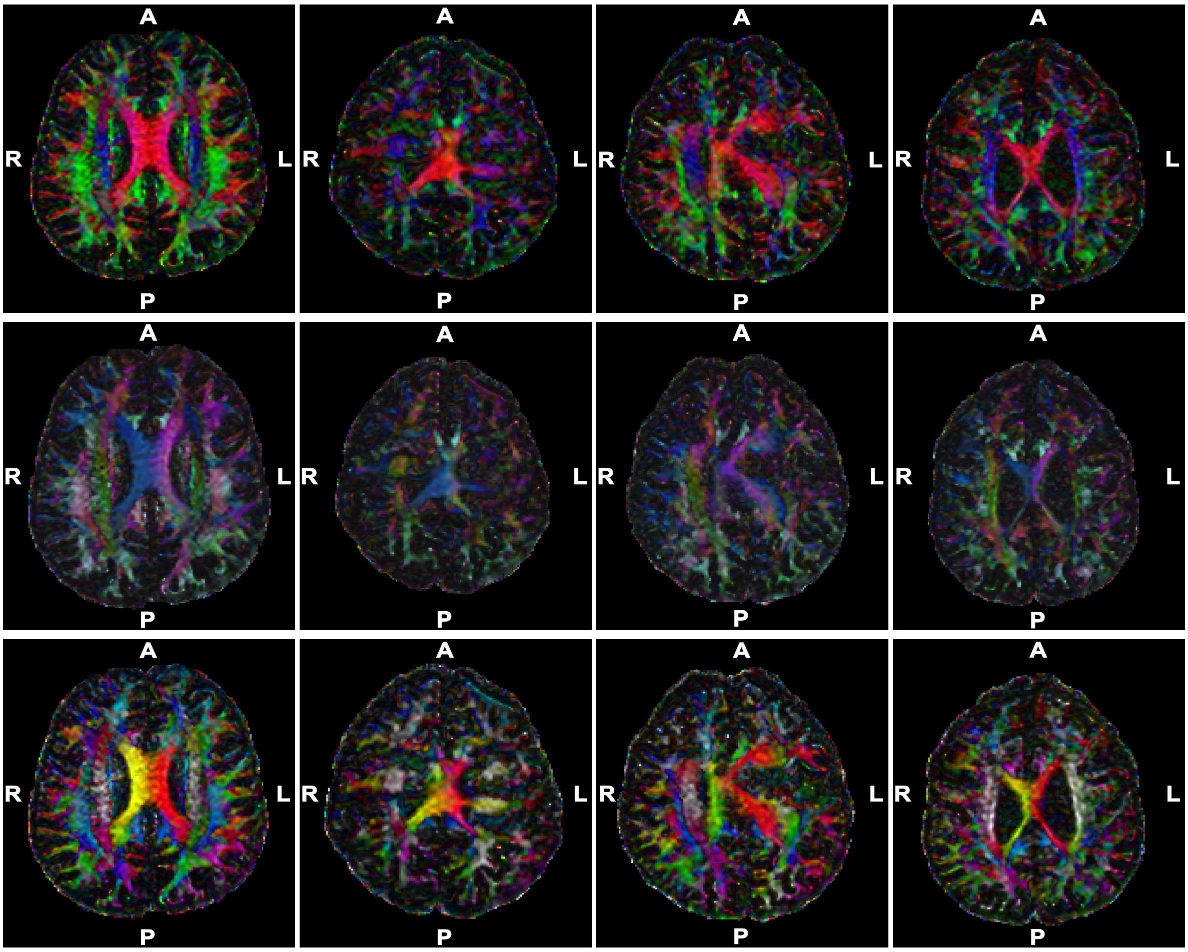

(a) (b) (c) (d)

Figure 12: Axial slices at the point of maximum anterior-to-posterior width of the corpus callosum: absolute value color scheme in the top row, Boy surface scheme in the middle row, and the proposed color scheme in the bottom row. As a reference, (a) shows a healthy control. The other columns (b)–(d) display slices from patients with brain malformations. The color patterns in the bottom row draw more attention to structural abnormalities.

Figure 12 provides a comparison of the results of the absolute value scheme (top row), those of the Boy surface scheme (middle row), and those of the proposed color scheme (bottom row) in the revelation of spatial orientation of the tract in the DTI exams of patients with subcortical band heterotopia. This congenital disease consists of a diffuse neuronal migration that leads to the anomalous presence of gray matter interspersed in the white matter. For comparison, the colored slices of a healthy control are shown in Figure 12(a). The proposed color scheme (bottom row) reveals more details than do the absolute value and Boy surface scheme, not only for the healthy control, but also when abnormalities are present. The abnormality is especially clear in the slice of the corpus callosum colored using the proposed scheme, where the fibers which should be running upwards (red and yellow in the normal brain) are revealed to be running in other directions (greenish and magenta). The spatial orientation of the superior longitudinal fasciculus is also more discernible with the proposed scheme than it is with the Boy surface scheme.

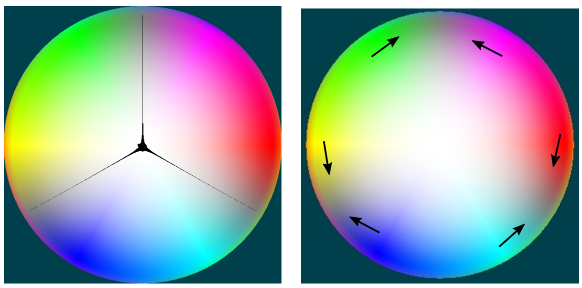

(a) (b)

Figure 13: Pitfalls of the proposed color scheme: (a) non-invertibility and (b) perceptually gray bands.

5. Discussion

This paper addresses the issue of the ambiguity found in the color coding of spatial line path and proposes a less ambiguous option. In order to assign distinctive and smoothly varying colors to line orientations, we propose a color wheel consisting of alternating primary and secondary colors as illustrated in Figure 4. When compared with previous research, the proposed color scheme furnishes a representation with a perceptually unambiguous line orientation without the artifact of discontinuity. Nevertheless, similar to the results with the Boy surface scheme, this mapping is not invertible for all colors. This is because in the interpolation of a primary color and a secondary color differing in three elements (such as red (1.0, 0.0, 0.0) and cyan (0.0, 1.0, 1.0)), the same gray values are obtained at three points along each latitude of the color sphere. All the orientations highlighted in black in Figure 13(a) are ambiguously mapped. Therefore, the proposed color scheme is not appropriate for interactions such as color picking for the identification of a specific orientation, although an evaluation of the colors in the vicinity of the ambiguous gray does provide a possible solution for distinguishing the coded orientations.

Although the linear interpolation of adjacent colors leads to the three gray bands on the color sphere indicated by the black arrows in Figure 13(b) can be argued to cause incorrect interpretation of line path, the consideration of these colors in conjunction with the adjacent ones leads to a different perception of the DTI images. Our explanation for these surprising results is that the appearance of a color is strongly dependent on its surroundings [19] and the smoothness of the geometry of tract.

To validate the proposed line-coding color scheme, both co-registered DTI and T1-weighted MRI images were used to ascertain the location of the uncinate fasciculus as it runs upwards from the temporal lobe to the insular cortex to form a spatial pathway that intersects the 2D slices under investigation diagonally, rather than transversely or longitudinally. Therefore, the many intersections are reduced to a set of points on the slices, which makes it difficult to identify the uncinate fasciculus in a slice-by-slice investigation. A 3D visualization, however, can help clarify the spatial orientation of these white matter tracts.

Despite the shortcomings in the color codes mentioned above, it is still widely used in data visualization, either because it approximates the physical spectrum of applications or has a direct correspondence to the vectors represented. The familiarity of 2D visualization makes combination with colored DTI volumes an interesting option for multimodal visualization. Far from providing an accurate visualization of spatial orientation, the proposed color scheme does provide a simple and rapid alternative furnishing more information about the orientation of fiber tracts than do the traditional color schemes.

The way to display the key for the color mapping of the path of a spatial line on a plane presents a challenge. This issue has also been addressed. Three colored sphere projections were investigated: stereographic projections (Figure 4), parallel ones (Figure 5(b)), and equirectangular ones (Figure 14). From our corridor testing, all three colormaps required extra mental effort for interpretation. Nevertheless, possibly because of our pre-attentive association of a disc-shaped figure with a sphere, it seems that the disc shape produces better spatial perception. The stereographic and parallel projections were found to be perceptually similar. Although equirectangular projection is not suitable as the key to color mapping, it is quite appropriate for texture lookup-based implementation. A comparison of the equirectangular projection of the proposed scheme in Figure 14(a) and that provided by the Boy surface scheme (Figure 14(b)) suggests that the proposed scheme is preferable in relation to color sequencing and richness of tone.

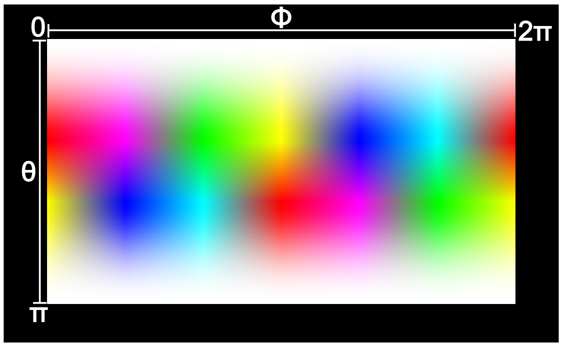

(a)

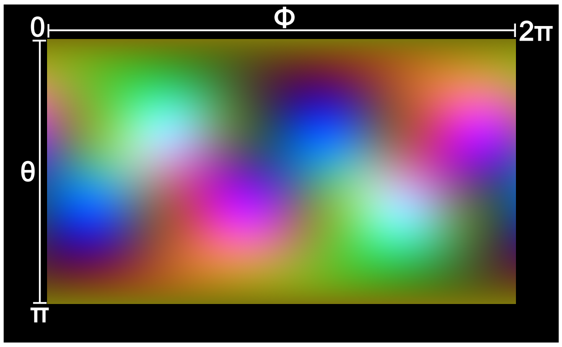

(b)

Figure 14: Equirectangular projection as the key to color mapping of line paths: (a) present proposal; (b) Boy surface scheme (available at [24]).

6. Concluding Remarks

Although the 3D rendering of fiber tracts has evolved rapidly, scalar indices such as fractional anisotropy (FA) and mean diffusivity (MD) are still the most widely used tools in the study of the microstructural properties of tissues. 2D visualization is familiar to radiologists, even though the path of fibers cannot be conveyed. Such information about orientation can be crucial for understanding the architecture of fibers, however, and a novel option has been proposed here, one based on a line-coding color scheme for displaying a fiber tract in 2D. A corridor test was performed to obtain the feedback of both physicians and non-physicians. All volunteers could distinguish correctly the direction of major diffusivity once the color display had been explained. Such a superficial approach, however, cannot demonstrate the true clinical value of the scheme. In the future, we plan to design an usability test for potential users who are familiar with DTI images to assess the utility of the proposed scheme.

As already discussed in Section 5, the proposed color coding scheme is not adequate for all studies of tract architecture, including the analysis of the symmetry of cerebral hemispheres. The proposed scheme is, however, a complementary scheme designed to facilitate the study of subtle variations in diffusivity in slice-by-slice exploration. We believe that, together with other vector color schemes and tractography, one can build a 3D exploratory visualization environment that supports the Visual Information Seeking Mantra [25]: (3D) Overview first, zoom and filter, then (2D) details-on-demand. Such a visual exploratory environment is our long-term goal.

Acknowledgements

The authors would like to acknowledge the contribution of Fernando Cendes in providing the MRI volume data and of Linda G. El-Dash in the proof-reading of the text. The research was supported by a CNPq-Brazil fellowship (305785/2012-5, 308764/2015-3), a CNPq-Brazil scholarship (153389/2014-1), and the Fapesp-Brazil grant #2013/07559-3 to the BRAINN Research, Innovation and Dissemination Center of the University of Campinas.

References

[1] Mori S, van Zijl PCM. Fiber tracking: principles and strategies - a technical review. NMR in Biomedicine 2002;15(7-8):468–80. URL: http://dx.doi.org/10.1002/nbm.781. doi:10.1002/nbm.781.

[2] Lerner A, Mogensen MA, Kim PE, Shiroishi MS, Hwang DH, Law M. Clinical applications of diffusion tensor imaging. World Neurosurgery 2014;82(1-2):96–109. URL: http://dx.doi.org/10.1016/j.wneu.2013.07.083. doi:10.1016/j.wneu.2013.07.083.

[3] Mori S, Zhang J. Principles of diffusion tensor imaging and its applications to basic neuroscience research. Neuron 2006;51(5):527–39. URL: http://dx.doi.org/10.1016/j.neuron.2006.08.012. doi:10.1016/j.neuron.2006.08.012.

[4] Kindlmann G. Superquadric tensor glyphs. In: Deussen O, Hansen C, Keim D, Saupe D, editors. Eurographics / IEEE VGTC Symposium on Visualization. Aire-la-Ville, Switzerland, Switzerland: The Eurographics Association. ISBN 3-905673-07-X; 2004, p. 147–54. URL: http://dx.doi.org/10.2312/VisSym/VisSym04/147-154. doi:10.2312/VisSym/VisSym04/147-154.

[5] Bihan DL, Mangin JF, Poupon C, Clark CA, Pappata S, Molko N, et al. Diffusion tensor imaging: Concepts and applications. J Magn Reson Imaging 2001;13(4):534–46. URL: http://dx.doi.org/10.1002/jmri.1076. doi:10.1002/jmri.1076.

[6] Jones DK, Travis AR, Eden G, Pierpaoli C, Basser PJ. PASTA: Pointwise assessment of streamline tractography attributes. Magnetic Resonance in Medicine 2005;53(6):1462–7. URL: http://dx.doi.org/10.1002/mrm.20484. doi:10.1002/mrm.20484.

[7] Vilanova A, Zhang S, Kindlmann G, Laidlaw D. An introduction to visualization of diffusion tensor imaging and its applications. In: Visualization and Image Processing of Tensor Fields. Springer-Verlag; 2006, p. 121–53. URL: http://dx.doi.org/10.1007/3-540-31272-2_7. doi:10.1007/3-540-31272-2_7.

[8] Preim B, Botha CP. Visual Computing for Medicine: Theory, Algorithms, and Applications. 2 ed.; San Francisco, CA, USA: Morgan Kaufmann Publishers Inc.; 2013. ISBN 9780124159792.

[9] Pajevic S, Pierpaoli C. Color schemes to represent the orientation of anisotropic tissues from diffusion tensor data: application to white matter fiber tract mapping in the human brain. Magnetic resonance in medicine 1999;42(3):526–40. URL: http://dx.doi.org/10.1002/(SICI)1522-2594(199909)-42:3<526::AID-MRM15>3.0.CO;2-J. doi:10.1002/(SICI)1522-2594(199909)42:3<526::AID-MRM15>3.0.CO;2-J.

[10] Engel K, Hadwiger M, Kniss J, Rezk-Salama C, Weiskopf D. Real-time Volume Graphics. Natick, MA, USA: A. K. Peters, Ltd.; 2006. ISBN 1568812663. URL: http://dx.doi.org/10.1201/b10629. doi:10.1201/b10629.

[11] Post FH, van Walsum T. Fluid flow visualization. In: Focus on Scientific Visualization. London, UK, UK: Springer-Verlag. ISBN 3-540-54940-4; 1993, p. 1–40. URL: http://dx.doi.org/10.1007/978-3-642-77165-1_1. doi:10.1007/978-3-642-77165-1_1.

[12] Smith AR. Color gamut transform pairs. ACM SIGGRAPH Computer Graphics 1978;12(3):12–9. URL: http://dx.doi.org/10.1145/965139.807361. doi:10.1145/965139.807361.

[13] Schlüter M, Stieltjes B, Rexilius J, Hahn H, Peitgen HO. Unique planar color coding of fiber bundles and its application to fiber integrity quantification. In: 2004 2nd IEEE International Symposium on Biomedical Imaging: Macro to Nano (IEEE Cat No. 04EX821); vol. 1. Institute of Electrical & Electronics Engineers (IEEE); 2004, p. 900–3. URL: http://dx.doi.org/10.1109/ISBI.2004.1398684. doi:10.1109/isbi.2004.1398684.

[14] Liu SX. Symmetry and asymmetry analysis and its implications to computer-aided diagnosis: A review of the literature. Journal of Biomedical Informatics 2009;42(6):1056–64. URL: http://dx.doi.org/10.1016/j.jbi.2009.07.003. doi:10.1016/j.jbi.2009.07.003.

[15] He R, Mehta M, Narayana P. Color coding for visualization of the directional information of DTI. In: The 26th Annual International Conference of the IEEE Engineering in Medicine and Biology Society; vol. 1. Institute of Electrical & Electronics Engineers (IEEE); 2004, p. 1857–9. URL: http://dx.doi.org/10.1109/IEMBS.2004.1403552. doi:10.1109/iembs.2004.1403552.

[16] Demiralp C, Hughes J, Laidlaw D. Coloring 3d line fields using boy's real projective plane immersion. IEEE Trans Visual Comput Graphics 2009;15(6):1457–64. URL: http://dx.doi.org/10.1109/tvcg.2009.125. doi:10.1109/tvcg.2009.125.

[17] Opensource . Diffusion mr imaging in python. 2016. URL: https://github.com/nipy/dipy/blob/master/dipy/viz/colormap.py; accessed in July 2016.

[18] Wideman G. Orientation and Voxel-Order Terminology: RAS, LAS, LPI, RPI, XYZ and All That. http://www.grahamwideman.com/gw/brain/orientation/orientterms.htm; 2016. Accessed in February 2016.

[19] Ware C. Color sequences for univariate maps: theory, experiments and principles. IEEE Comput Grap Appl 1988;8(5):41–9. URL: http://dx.doi.org/10.1109/38.7760. doi:10.1109/38.7760.

[20] Pierpaoli C, Basser PJ. Toward a quantitative assessment of diffusion anisotropy. Magn Reson Med 1996;36(6):893–906.

[21] FMRIB . FMRIB's Diffusion Toolbox. 2016. URL: http://fsl.fmrib.ox.ac.uk/fsl/fslwiki/FDT; accessed in February 2016.

[22] NEMA . DICOM – Digital Imaging and Communications in Medicine. 2016. URL: http://dicom.nema.org/; accessed in February 2016.

[23] DCM2NII . dcm2nii DICOM to NIfTI conversion. 2016. URL: http://www.mccauslandcenter.sc.edu/mricro/mricron/dcm2nii.html; accessed in February 2016.

[24] Voltoline R. Multimodal visualization of diffusion tensor imaging. 2016. URL: http://www.dca.fee.unicamp.br/projects/mtk/voltoline/download.html; accessed in July 2016.

[25] Shneiderman B. The eyes have it: a task by data type taxonomy for information visualizations. In: Proceedings 1996 IEEE Symposium on Visual Languages. VL '96; Washington, DC, USA: Institute of Electrical & Electronics Engineers (IEEE). ISBN 0-8186-7508-X; 1996, p. 336–43. URL: http://dx.doi.org/10.1109/VL.1996.545307. doi:10.1109/vl.1996.545307.